

Measurement of Rabbit Eardrum Vibration through Stroboscopic Digital Holography

Daniël De Greef^a and Joris J. J. Dirckx^a

^a *University of Antwerp, Laboratory of BioMedical Physics, Groenenborgerlaan 171, B-2020 Antwerp, Belgium*

Abstract. In this work, we present a setup for high-power single shot stroboscopic digital holography and demonstrate it in an application on rabbit eardrum vibration measurement. The setup is able to make full-field time-resolved measurements of vibrating surfaces with a precision in the nanometer range in a broad frequency range. The height displacement of the measured object is visualized over the entire surface as a function of time. Vibration magnitude and phase maps can be extracted from these data, the latter proving to be very useful to reveal phase delays across the surface. Such deviations from modal motion indicate energy losses due to internal damping, in contrast to purely elastic mechanics. This is of great interest in middle ear mechanics and finite element modelling.

In our setup, short laser pulses are fired at selected instants within the surface vibration period and are recorded by a CCD camera. The timing of the pulses and the exposure of the camera are synchronized to the vibration phase by a microprocessor. The high-power frequency-doubled Nd:YAG laser produces pulses containing up to 5 mJ of energy, which is amply sufficient to record single-shot holograms. As the laser pulse length is 8 ns and the smallest time step of the trigger electronics is 1 μ s, vibration measurements of frequencies up to 250 kHz are achievable through this method, provided that the maximum vibration amplitude exceeds a few nanometers. In our application, middle ear mechanics, measuring frequencies extend from 5 Hz to 20 kHz.

The experimental setup will be presented, as well as results of measurements on a stretched circular rubber membrane and a rabbit's eardrum. Two of the challenges when measuring biological tissues, such as the eardrum, are low reflectivity and fast dehydration. To increase reflectivity, a coating is applied and to counteract the undesirable effects of tissue dehydration, the measurement setup and software have been optimized for speed without compromising on the quality. Results of a repeatability test will be presented as well.

Since the method measures the membrane motion as a function of time in small time steps, we do not only measure vibration amplitude like in time-average holography, but we can also measure non-linear elastic and transient behaviour. In conclusion, the combination of good spatial, depth and time resolution with the fast data acquisition and very wide frequency range make our technique applicable in a number of fields, including biological tissue vibrations.

1. INTRODUCTION

Digital holography is a powerful and versatile full-field measuring technique that is able to measure nanometer scale displacements of surfaces. The technique has become increasingly useful with the rise of commercially available high-resolution cameras. Middle ear biomechanics is one example of a research field that can benefit from digital holography [1,2,3]. Knowledge of the response of the middle ear components to an incident sound wave is of capital importance in a full understanding of the middle ear system as an impedance match between sound waves in air and in the cochlear fluid in the inner ear. In the past, the motion of middle ear structures has been visualized for different frequency and displacement ranges by a multitude of non-contact measurement techniques, including single point or scanning LDV [4], X-ray stereoscopy [5], time-average holography [1,6] and double-exposure holography [7,8]. In recent years, stroboscopic digital holography was introduced the field as it provides full-field time-resolved displacement data over the full acoustic frequency range with a high temporal, spatial and depth resolution, which is unmatched by any of the other techniques [2,3].

In this work, our new setup for digital stroboscopic holography is presented. This setup includes a high-energy pulsed laser and highly precise trigger electronics which allow the recording of holograms at chosen time instants in the vibration period. Thanks to this, a wider frequency range than in previous similar setups is measurable, ranging from quasi-static to high-acoustic frequencies. Results are presented on a test sample for a range from 5 Hz to 16.7 kHz and on a rabbit eardrum for relevant acoustic frequencies, as well as results of a repeatability test of the technique. We also compare it to other techniques, and discuss applications and future plans.

2. METHOD

2.1 Digital Holography

In digital holography, interference patterns of mutually coherent object and reference beams are recorded on a digital imaging matrix, such as a CCD or a CMOS. After numerical reconstruction the optical phase information of the object wave is directly accessible, allowing the acquirement of an objects displacement between to recorded states. This is achieved by subtracting the two reconstructed phase maps of the two respective holograms. As a result, a wrapped phase difference map is obtained. This can be converted into a displacement map of the deformation along the setup's sensitivity vector, by applying a two-dimensional phase unwrapping algorithm. The chosen hologram reconstruction algorithm for in this work is the central reconstruction formula of digital holography [9], achieved by applying the Fresnel approximation to the Fresnel-Kirchhoff transform integral:

$$b(n\Delta x, m\Delta y) = e^{i\pi d\lambda\left(\frac{n^2}{N^2\Delta\xi^2} + \frac{m^2}{M^2\Delta\eta^2}\right)} \sum_{k=0}^{N-1} \sum_{l=0}^{M-1} h(k, l) r^*(k, l) e^{\frac{i\pi}{d\lambda}(k^2\Delta\xi^2 + l^2\Delta\eta^2)} e^{-2i\pi\left(\frac{kn}{N} + \frac{lm}{M}\right)} \quad (1)$$

with b the reconstructed complex object wave; n, m the image indices; $\Delta x, \Delta y$ the image pixel center-to-center distances; d the chosen reconstruction distance; λ the optical wavelength of the laser; $\Delta\xi, \Delta\eta$ the CCD pixel distances; N, M the number of pixels in x - and y -direction; k, l the CCD indices; h the recorded hologram and r^* the conjugated reference wave.

2.2 Stroboscopic Digital Holography

In order to measure vibrations using digital holography, several options are available, including time-average [10] and double-exposure holography [11]. However, in recent years, stroboscopic digital holography has proven to provide the best information of the available holography based alternatives for vibrometry in terms of quantity and quality [2,3]. In stroboscopic digital holography, the object is illuminated using one or multiple very short pulses, synchronized to a single vibration phase. After combining it with a hologram of the object in rest, the absolute displacement map of the vibrating object can be deducted. When these pulses are subsequently cycled stepwise through the entire vibration period, displacement maps for evenly distributed time instants within the vibration period are collected. Therefore, the full-field deformation of the objects surface is obtained as a function of time with a temporal resolution that is only limited by the pulse length of the laser and the precision of the triggering. This can reveal non-modal components in the motion that are not predicted by theory.

2.3 Setup

An overview of the setup is depicted in Fig. 1. A frequency doubled pulsed Nd:YAG laser (JK Lasers, $\lambda = 532$ nm), produces pulses of up to 5 mJ with a duration of 8 ns. A Galilean beam expander (GBE) makes the beam wider and a $\lambda/2$ -plate manipulates the light polarization. After this, the beam is divided into an object and reference beam (OB and RB) by a polarizing beam splitter (PBS). The OB is partially reflected by a non-polarizing beam splitter (NPBS 1), directing it perpendicularly towards the recorded object. The object's surface reflects the OB back through the NPBS 1 towards NPBS 2, where it is combined with the unaltered RB. Their interference pattern is recorded by a commercial CCD camera (AVT Pike 505-B, 2452x2054, 14bit). A piece of custom made electronics, combined with two arbitrary function generators (AFG) control the precise triggering of the laser and the camera, both synchronized to each other and to the sound excitation. Details of the triggering system will be published soon by the same first author as this text.

For measurements of acoustically stimulated motion in general and eardrum vibration in particular, an acoustic stimulation element (ASE) was designed and constructed. The ASE is a rigid tube with at one end an opening for the studied object and at the other end an oblique window. This window prevents the sound energy from escaping from this side, while allowing the object beam to illuminate the object. Because the window is attached under an angle, unwanted reflections into the optical path are avoided. The wall of the ASE provides access for a speaker signal and a probe tube microphone (Bruel & Kjaer 4182). This probe microphone measures both sound intensity and phase.

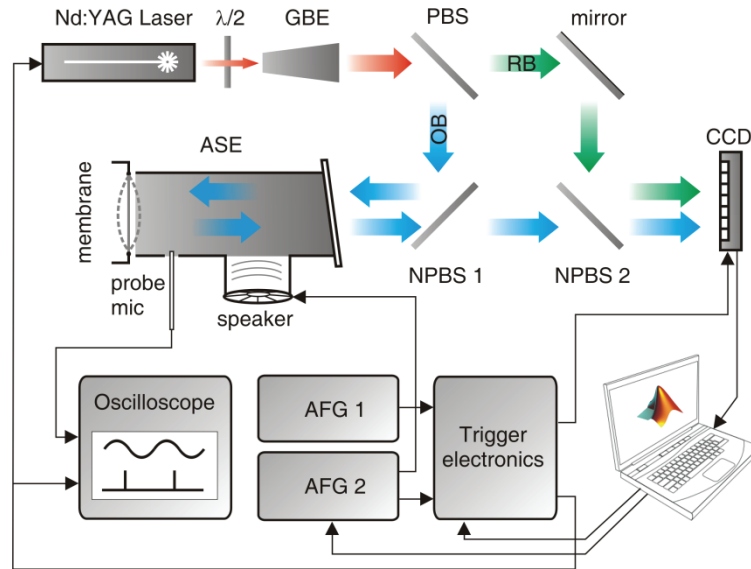


FIGURE 1. Overview of the setup for digital holography. GBE: Galilean beam expander, (N)PBS: (Non-)polarizing beamsplitter, OB: Object beam, RB: Reference beam, ASE: Acoustic stimulation element, AFG: Arbitrary function generator.

2.4 Rabbit Sample Preparation

A male New-Zealand White rabbit of 12 weeks old, often used in the main research line of our group, was euthanized by natriumpentobarbital injections (DOLETHAL (Vétoquinol) 200 mg/ml) at the pinna which was locally anesthetized with Xylocaine. All animal manipulations in this work were performed in accordance with Belgian legislation and the directives set by the Ethical committee on Animal Experimentation of our institution (University of Antwerp, Belgium). After euthanasia, the animal was decapitated and the bulla was removed from the skull to gain access to middle ear. In order to make the tympanic membrane fully visible, the entire bony ear canal was drilled away. The tympanic membrane was painted using a thin layer of a 5% TiO₂ suspension in deionized water to counteract the low reflectivity of the eardrum. During the entire preparation, the sample was kept moist by exposing it to a humidifier (Bionaire) to minimize fast dehydration and its influence on elastic parameters.

The measurement system has been optimized for fast acquisition, allowing a full-spectrum vibration measurement of 41 frequencies ranging from 25 Hz to 25600 Hz at 4 frequency steps per octave, at 8 vibration holograms plus 1 reference frame per frequency within 15 minutes after the end of preparation, with the actual measurement taking less than 3 minutes. This is of major importance in measurement of biological tissue, which is very sensitive to post-mortem dehydration effects.

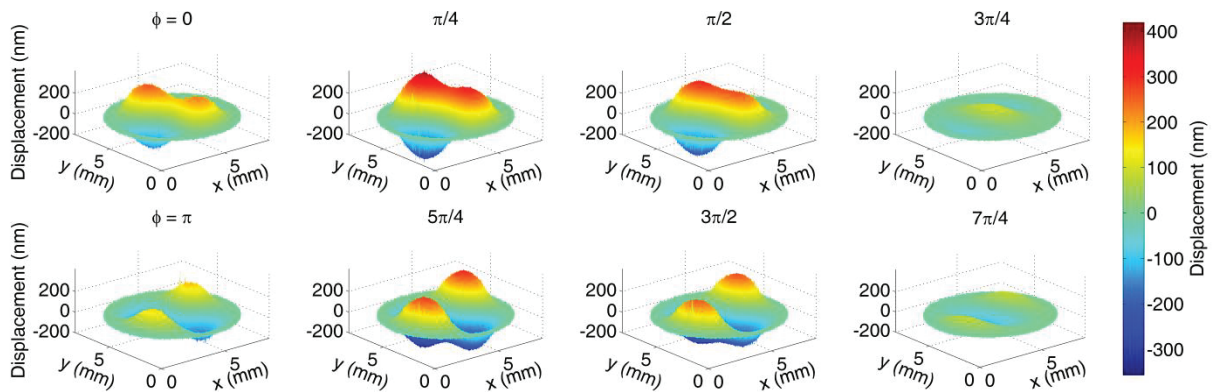


FIGURE 2. Displacement maps of a stretched rubber membrane, acoustically stimulated at a frequency of 3805.5 Hz and a sound pressure of 100 dB SPL.

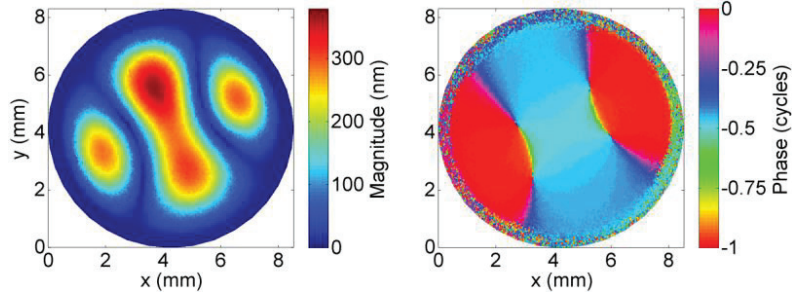


FIGURE 3. Full-field transfer function magnitude (left) and phase (right) maps of a stretched rubber membrane, 3805.5 Hz, 100 dB SPL. Data extracted from the same measurements as Fig. 2.

3. RESULTS

3.1 Membrane vibration

Figures 2, 3 and 4 present results of a measurement on a test object, in this case a stretched rubber membrane with a diameter of 8 mm. Figure 2 shows eight displacement maps of the membrane, excited at 3805.5 Hz with a sound pressure of 100 dB SPL. In order to extract full-field magnitude and phase information of the membrane's transfer function, the complex FFT-spectrum of the temporal displacement for every object point was calculated. The magnitude and phase of the principal vibration component are calculated and presented for every object point of the membrane in Fig. 3 (left: magnitude map, right: phase map). The phase map presents the displacement phase relative to the acoustic stimulus phase. Four separate local maxima are visible on the magnitude map, while on the phase map continuous phase transitions are noticed over the entire membrane.

Figure 4 presents magnitude and phase maps of four more vibrational patterns. The stimulation frequencies range from 5 Hz to 16.7 kHz. This shows that the developed setup produces good results for a very wide frequency range. At 5 Hz, the membrane does not vibrate exactly in phase with the sound wave. This is presumably caused by the viscoelastic nature of the material. At frequencies closer to but below the resonance frequency (cfr. 1903 Hz in Fig. 4), the membrane moves exactly in phase with the sound stimulus, indicated by the red color. At higher frequencies, many instances of continuous phase transitions can be observed, indicating non-modal behavior.

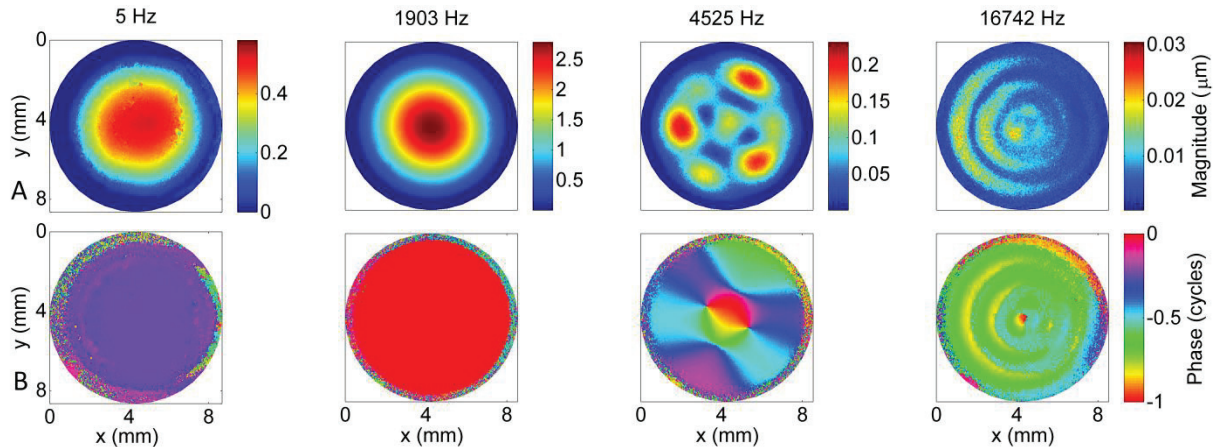


FIGURE 4. A. Magnitude maps and B. phase maps of a vibrating membrane at different frequencies covering the entire range of our setup and the chosen test sample. The applied sound pressure values are 90 dB SPL for 5 Hz, 95 dB SPL for 1.9 kHz, 100 dB SPL for 4.5 kHz and 95 dB SPL for 16.7 kHz.

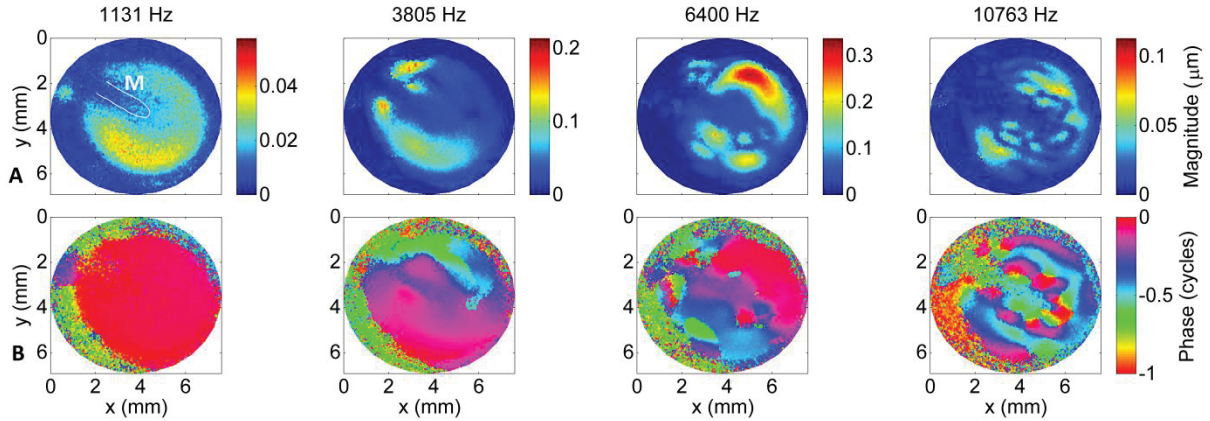


FIGURE 5. Magnitude maps and B. phase maps of a rabbit eardrum for relevant acoustic frequencies. The applied sound pressure values are 100 dB SPL for 1.1 kHz, 105 dB SPL for 3.8 kHz, 105 dB SPL for 6.4 kHz and 85 dB SPL for 10.8 kHz. The position of the malleus is indicated by a white line and ‘M’ in the first image and is unchanged in the others.

3.2 Eardrum Vibration

The magnitude and phase maps of four different vibration measurements on a rabbit eardrum are presented in Fig. 5. The frequencies were chosen to be representative of the vibration features in each frequency range and are 1131 Hz, 3805 Hz, 6400 Hz and 10763 Hz. The location of the arm of the malleus (the first of three small ossicles which transport sound energy from the eardrum to the inner ear) is indicated by a white line and capital ‘M’ in the first image and is consistently at the same location in the other images.

It is clear that the attachment to the malleus reduces the magnitude and reduces phase variations along this attachment, even at higher frequencies. Furthermore, one can notice a gradual increase in pattern complexity with increasing frequency and multiple vibration maxima that are ordered radially around the tip of the malleus at the highest frequency. Similarly to the results for the test membrane, continuous phase variations are observed, contradicting purely modal patterns that were assumed in earlier literature about eardrum vibrations [6], and thus indicate viscoelastic properties of the membrane.

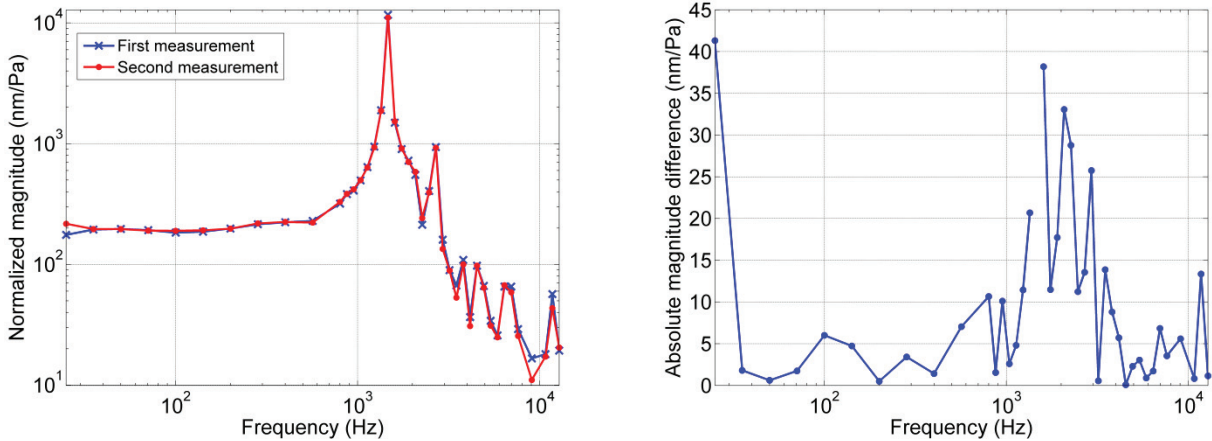


FIGURE 6. Left: Transfer function magnitude results from two full-spectrum repeatability tests. Right: Absolute value of the normalized magnitude difference between the repeated measurements. Results are extracted from the center point a vibrating rubber membrane. In between measurements, an interval of 3 minutes was left.

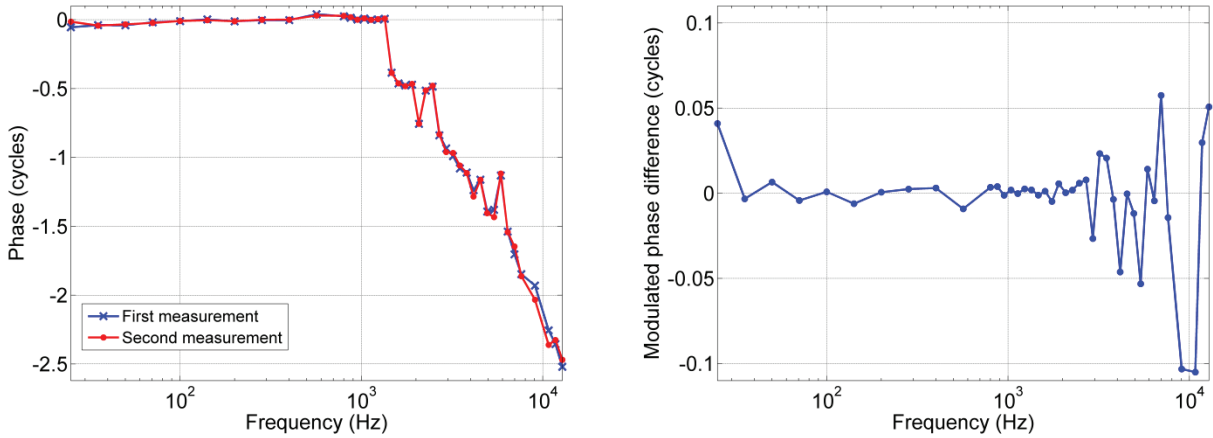


FIGURE 7. Left: Transfer function phase results from the two full-spectrum repeatability tests. These figures originate from the same data as Fig. 6. Right: Modulated phase difference between the repeated measurements.

3.3 Repeatability Test

In order to evaluate the repeatability of the technique, we carried out a repeated full-spectrum analysis of a membrane using the same input stimuli at the same frequencies with an interval of 3 minutes between measurements. None of the recording parameters and circumstances was changed in between measurements. The results of the repeatability measurements are presented in Fig. 6 (magnitude) and Fig. 7 (phase), where the frequency-dependent transfer function of the center point of the membrane is shown.

At most frequencies below 1200 Hz and above 2000 Hz, the absolute magnitude difference between measurements is well below 10nm. As can be expected, difference values are higher in ranges where the transfer function has large values and steep tangents, i.e. close to the sample's resonance frequency. Note that these data were extracted from a single data point and that neither smoothing nor averaging has been applied to reduce noise effects.

The modulated phase difference in Fig. 7 (right) is defined as:

$$p_{diff} = \begin{cases} \text{mod}(p_2 - p_1, 1) & \text{if } < 0.5 \\ \text{mod}(p_2 - p_1, 1) - 1 & \text{if } > 0.5 \end{cases} \quad (2)$$

with p_1 and p_2 being the frequency dependent phase from the first and second measurement, respectively. The absolute value of the modulated phase difference is well below 0.05 cycles for most frequencies below 7 kHz and is more variable for values above 7 kHz. At these high frequencies, however, very small errors in time measurement can lead to considerable differences in phase.

4. DISCUSSION

The ability to gather time-resolved vibrational information over entire surfaces with an excellent spatial resolution is a large advantage over single-point techniques such as LDV, which require extensive scanning procedures to cover surfaces. On the other hand, as holography measures displacement rather than velocity, it is sensitive to uncontrolled (quasi-)static motions in between measurement pulses. Therefore, LDV and digital stroboscopic holography can be used complementary, as shown in an application on avian middle ears in [12] (in this issue).

Similar setups to the one presented in this work use chopped continuous lasers [2,3], resulting in lower energy pulses compared to our setup, in which a high-energy pulsed laser has been incorporated. In order to collect a sufficient amount of light on the CCD using the lower power pulses, longer pulse lengths are needed (10 % of the vibration period) and a number of these pulses need to be integrated, causing a threefold disadvantage compared to our setup. Firstly, since the illumination length is 10% of the vibration period, different positions of the object in time will contribute to the recorded interferogram, causing in a loss of resolution. Secondly, as the pulse length increases for decreasing frequency, stability problems arise in the low-frequency range, resulting in a low-frequency limit of 200 Hz in the published results. Thirdly, the capability of recording single-shot holograms with an ultra-

short single laser pulse enables us to extend the technique to measurement of extremely fast transient events with a sub-microsecond temporal resolution, which is not possible with other published setups.

As already mentioned, our lab uses the technique to study the motion of the eardrum in mammals but also in avian species, as presented in [12]. However, it can be used in other fields than biomechanics where full-field vibration information in a frequency range from 1 Hz to 250 kHz could contain value.

In the future, the setup will be further optimized to measure very rapid transient motions. This will provide new information of major importance that will be used to characterize viscoelastic behavior of materials or to study the propagation of traveling waves. Since the laser pulses in our current setup have a duration of merely 8 ns and one pulse contains sufficient energy to record a hologram, very rapid transient motions can be visualized with a temporal resolution of 1 μ s, which currently is the smallest time step on our microchip's program. The setup could be able to measure transient motions with a sub-microsecond temporal resolution after further optimization of the triggering electronics. Note that the transient phenomenon needs to be reproducible, as the different holograms cannot be recorded during a single event.

5. CONCLUSION

In this paper, we presented the concept and practical details of our setup for digital stroboscopic holography. The setup incorporates dedicated triggering electronics and a high-energy pulsed laser, allowing full-field time-resolved imaging of periodical displacements in the nanometer range for frequencies extending from quasi-static to high acoustic frequencies. Results are presented on a test sample for 5 Hz to 16.7 kHz. Furthermore, the application of the technique on a biomechanical sample, more specifically a rabbit eardrum, was explained and results are presented for relevant acoustic frequencies. To assess the reliability of the technique, a repeatability test was carried out and results of this are shown as well. Finally the relevance of the setup was discussed in the light of complementary or similar setups, applications and future plans.

ACKNOWLEDGMENTS

This work was financially supported by the Research Foundation Flanders (FWO) and the University of Antwerp. We thank W. Deblauwe and F. Wiese for their technical support.

REFERENCES

1. J.J. Rosowski, J.T. Cheng, M.E. Ravicz, N. Hulli, M. del S. Hernandez-Montes, and E. Harrington, *Hear. Res.* **253**, 83 (2009).
2. J.T. Cheng, A.A. Aarnisalo, E. Harrington, M. del S. Hernandez-Montes, C. Furlong, S.N. Merchant, and J.J. Rosowski, *Hear. Res.* **263**, 66 (2010).
3. D. De Greef, J. Aernouts, J. Aerts, J.T. Cheng, R. Horwitz, J.J. Rosowski, and J.J.J. Dirckx, "Viscoelastic properties of the human tympanic membrane studied with stroboscopic holography and finite element modeling," *Hear. Res.* (2014). (submitted, DOI: 10.1016/j.heares.2014.03.002)
4. O. De La Rochefoucauld and E.S. Olson, *Hear. Res.* **263**, 9 (2010).
5. W.H.M. Salih, J. a M. Soons, and J.J.J. Dirckx, *Meas. Sci. Technol.* **22**, 025502 (7pp) (2011).
6. J. Tonndorf and S.M. Khanna, *J. Acoust. Soc. Am.* **52**, 1221 (1972).
7. C. Furlong, J.J. Rosowski, N. Hulli, and M.E. Ravicz, *Strain* **45**, 301 (2009).
8. M. del S. Hernandez-Montes, C. Furlong, J.J. Rosowski, N. Hulli, E. Harrington, J.T. Cheng, M.E. Ravicz, and F.M. Santoyo, *J. Biomed. Opt.* **14**, 034023 (2009).
9. T. Kreis, *Handbook of Holographic Interferometry* (Wiley-VCH Verlag GmbH & Co. KGaA, Weinheim, FRG, 2005), p. 542.
10. R.L. Powell and K.A. Stetson, *J. Opt. Soc. Am.* **55**, 1593 (1965).
11. P. Hariharan and B.F. Oreb, *Opt. Commun.* **59**, 83 (1986).
12. P. Muyshondt, D. De Greef, J. Soons, J. J. J. Dirckx, "Stroboscopic digital holography as validation tool for finite element modelling of biomechanical structures, demonstrated in bird ear research", *AIP Proceedings*, this issue (2014)

AIP Conference Proceedings is copyrighted by AIP Publishing LLC (AIP). Reuse of AIP content is subject to the terms at: <http://scitation.aip.org/termsconditions>. For more information, see <http://publishing.aip.org/authors/rights-and-permissions>.